Journal of Computer Engineering
ISSN 10003428

Original Research Article
Vol 11, Issue 9, 2022 | ISSN: 1000-3428

Novel Synthesis and Physicochemical Characterization of Rare-Earth Perovskite Nanoparticles via Coprecipitation Method

Muhammad A. Ridwan, Diana L. Sari, Rachmat S. Budiman, Hartati A. Wulan, Nurul F. Kurniawan

1Department of Chemistry, Universitas Negeri Yogyakarta, Yogyakarta, 55281, Indonesia

Abstract This study aims to synthesize $NdNiO_3$ perovskite nanoparticles calcined at different temperatures via coprecipitation method in the presence of sodium hydroxide as a precipitating agent and polyethylene glycol as a surfactant. The products are characterized by X-ray diffraction (XRD), Fourier transform infrared (FTIR), and Surface area analyzer (SAA). The phase composition by XRD indicates that $NdNiO_3$ is formed at 900 °C. The crystallite size using Scherrer equation shows crystallite size of $NdNiO_3$ in ranging of 44–72 nm. The FTIR spectra indicates O–Ni–O vibration led to $NdNiO_3$, in products calcined at 900 °C, with the wavenumber of 634 cm^{-1}. The $NdNiO_3$ exhibits a BET surface area of 133.79 m^2 g^{-1} and a BJH pore volume of 0.121 cc g^{-1} with the average particle size of 14.10 nm. All results show that the synthesis of $NdNiO_3$ via coprecipitation method is a suitable method to produce fine surfaces and pores with nanosized particles.

Introduction

Neodymium nickel oxide ($NdNiO_3$) is an oxide compound which has a perovskite-type structure ABO_3 (where A = rare-earth cation, B = transition metal cation). This compound has excellent crystallinity, surface area, and particle size characteristics. $NdNiO_3$ exhibits interesting structural [1], morphological [2], optical [3], electrical [4], magnetic, electronic [5], electrocatalytic [6], and transport [7] properties. Relating to these properties, the perovskite nanoparticles widely attract very interesting material due to its many applications especially in the renewable and sustainable energy point of view. The perovskite materials can be used as CO gas sensor [8], non-enzymatic glucose sensor [9], SOFC cathode material [10], enzyme mimetics [11], cathode catalyst for a borohydride fuel cell [12], gate dielectric material [13], supercapacitor electrode [14], and certainly active layer for a perovskite solar cell [15,16].

Different preparation methods of the perovskite oxides result in different physical or even chemical properties of materials [17]. A variety of methods are used to obtain nanoparticles with high homogeneity, purity, and nanosized particles as good as possible. Several methods have been studied for synthesizing $NdNiO_3$ perovskite nanoparticles, such as low-temperature [4], low temperature molten salt [18], decomposition [5], facile hydrothermal [9], sol-gel [19], pechini [20], soft post deposition annealing [21], gelatin [22], and citrate [23].

How to cite: Muhammad A. Ridwan, Diana L. Sari, Rachmat S. Budiman, Hartati A. Wulan, Nurul F. Kurniawan (2022). Novel Synthesis and Physicochemical Characterization of Rare-Earth Perovskite Nanoparticles via Coprecipitation Method. Journal of Computer Engineering, 11(9), 61–72. DOI: https://doi.org/10.5281/zenodo.19346154

Many soft chemical routes have been attempted, but there are no studies have been investigated for synthesizing $NdNiO_3$ using coprecipitation method. Hence, an attempt has been investigated on the synthesis and characterization of NdNiO3 perovskite nanoparticles by this method. Coprecipitation is the most convenient and common method for synthesizing perovskite nanoparticles. It was applied by several studies to prepare the nanoparticles, such as $LaNiO_3$ [14], $LaFeO_3$ [24], $LaCoO_3$ [25], $LaMnO_3$ [26], $LaAlO_3$ [27], $GdMnO_3$ [28], and $NdFeO_3$ [29]. There are very rare for synthesizing perovskite nanoparticles with rare earth cation of neodymium (Nd).

Coprecipitation exhibits the characteristics: the products are generally obtained as an insoluble species under supersaturation conditions; nucleation process forms a large number of small particles; post nucleation process as well as Ostwald ripening and aggregation, dramatically affects the size, morphology, and properties of the products; and the supersaturation conditions helps to induce precipitation at the result of a chemical reaction [30]. The advantages of this method are the high yield, high product purity, the lack of necessity to use organic solvents, easily reproducible, and low cost [31,32]. However, the properties of the obtained particles, such as size, shape, and composition are highly dependent on the reaction parameters (temperature, pH, ionic strength, kind of basic solution, and so on) [33]. In addition, perovskite nanoparticles obtained by this method are often not stable and hence are stabilized by using surfactant.

Generally, the starting materials for coprecipitation method are inorganic compounds such as metal nitrates, sulfates, and chlorides, which are blended under continuous stirring with one more required material than its precursors, a precipitating agent, and one supported material, a surfactant. Furthermore, coprecipitation is also an easier method than the others to prepare perovskite oxides because the precipitating agent can control chemical composition more quantitatively.

In this present work, the study aims to investigate that, for the first time, $NdNiO_3$ perovskite nanoparticles can be synthesized using coprecipitation method, starting from neodymium and nickel nitrates precursors. Furthermore, we will call the $NdNiO_3$ calcined at different temperatures, for the subsequent discussion. The characterizations verify the effect of the calcination temperature parameter on the particle size and surface area characteristics. These are considered important due to their effects in the crystallite structure which affect their performance as the functional materials.

Materials and Methods Materials

All of the chemicals were analytical grade. Neodymium nitrate hexahydrate ($Nd(NO_3)_3{\cdot}6H_2O$) and nickel nitrate hexahydrate ($Ni(NO_3)_2{\cdot}6H_2O$) were purchased from Merck. Polyethylene glycol 400 (PEG 400) and sodium hydroxide (NaOH) were obtained from Sigma-Aldrich. All chemicals were used as per received without any further purification. Distilled water was used in all experiments.

Synthesis Approach

In this work, $NdNiO_3$ perovskite nanoparticles were synthesized using coprecipitation method as follows. The synthesis was adopted with some modifications to previous study on the synthesis of $NdFeO_3$ nanocrystals [29]. In a typical synthesis, the overall stoichiometry should be in a ratio of 1:1 for Nd:Ni to obtain ABO_3 perovskite-type structure. First, 0.291 g (1 mmol) $Nd(NO_3)_2{\cdot}6H_2O$ and 0.438 g (1 mmol) $Ni(NO_3)_2{\cdot}6H_2O$ were each dissolved into 10 mL of distilled water. Both solutions were mixed together to prepare a precursor solution, followed by the addition of a

specified amount of PEG 400 as a surfactant. Then, aqueous solution of 1.5 M of NaOH was rapidly added to a precursor solution drop-wise. Adjusting NaOH as a precipitating agent was monitored until the solution reaches pH level of 7–8. The reaction was carried out under continuous stirring at 80 °C maintained constant for 1 h to obtain the final product. The precipitate was then separated from the final product by centrifugation and washed twice with distilled water and ethanol several times, and then oven-dried at 100 °C for 2 h. The oven-drying was succeeded by heat treatment with increasing the temperature at a rate of 10 °C min^{-1} to different temperatures, 700 °C and 900 °C, and the product was calcined at these temperatures for 4 h to obtain the $NdNiO_3$ perovskite phase.

The flow chart of $NdNiO_3$ perovskite nanoparticles synthesis using coprecipitation method was shown in Figure 1.

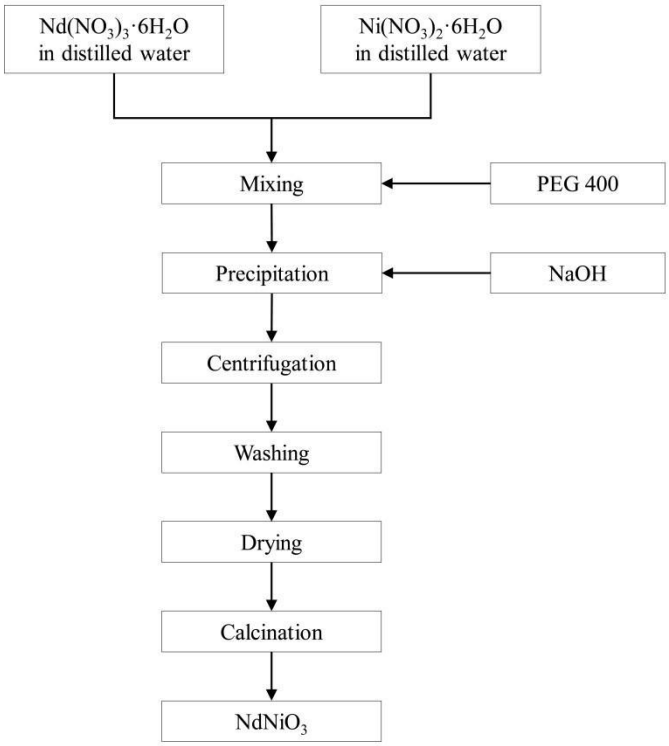

Figure 1: Schematic synthesis of $NdNiO_3$ perovskite nanoparticles prepared by co-precipitation method

Characterization

The crystalline nature of the products was determined by X-ray diffraction (XRD) patterns recorded using a

PANalytical Empyrean XRD diffractometer, over the range of 2θ = 10° to 90° with a step size of 0.026° and a counting time of 22 s per step. The system operated at 30 mA and 40 kV employing the X-ray wavelength of λ =

1.541 Å with a monochromated Kα radiation, emitted by Cu. The XRD diffractogram patterns were analyzed using X'Pert High Score Plus software to identify the composition phase performed using search and match method by comparing the patterns to those of the standards in the Inorganic Crystal Structure Database (ICSD) files. The crystallite size was calculated using Debye-Scherrer method (Equation 1). It is used to estimate the size of very small crystals from the measured width of their diffraction curves [34].

$$D = \frac{K\lambda}{\beta \cos\theta_B} \quad (1)$$

Where D is the crystallite size (nm), K is shape factor which is a typical value of about 0.9 but may vary depends on the actual shape of the crystallites assumed to be in the sample. The λ is the X-ray wavelength used (Cu/Kα = 0.154 nm), β is the line broadening at half the maximum intensity (FWHM) after subtracting the instrumental line broadening in radians, and θ_B is the Bragg angle obtained by dividing by 2 the 2θ value of the corresponding peak. The Fourier transform infrared (FTIR) was used to detect the functional groups presenting in the products. The spectra were recorded on a Nicolet iS50 FTIR spectrometer performed in the wavenumber interval of 4000 to 500 cm^{-1}. To record the spectra, the spectrometer supported a feature of Attenuated total reflectance (ATR) technique which enables samples to be examined directly as synthesized in the solid or liquid phase without any further preparation. The analysis was carried out by comparing the spectra for authentic drug samples and conjugated samples, then predict the possible conjugating sites. The difference of these spectra gave information about corresponding functional group.

The surface area and pore volume were analyzed by Quantachrome's Quadrasorb EVO surface area analyzer (SAA) and performed by Quantachrome QuadraWin software with nitrogen sorption isotherm technique. The samples were firstly degassed at 300 °C for 3 h before the measurement to eliminate the physically adsorbed water and other impurities. Nitrogen gas, as adsorbate, was performed on a SSA at a bath temperature of 77 K (the same temperature as the liquid nitrogen). The Brunauer-Emmett-Teller (BET) method was used to measure the specific surface area of each sample [35], while the pore size distribution was measured by Barrett-Joyner-Halenda (BJH) method [36].

Results & Discussion

Synthesis

In this work, the route of reactions used coprecipitation method to synthesize $NdNiO_3$ perovskite nanoparticles. Distilled water was used as the solvent in order to avoid the production of impurities in the final product. Addition of PEG 400, as a surfactant, when mixing the neodymium and nickel nitrate solutions is to reduce the size as well as improve the dispersibility. As reported by Damisih et al. [37], the particle size analysis exhibits decreasing of particle diameter as the addition of PEG surfactant. Their work confirmed that the addition of PEG 400 surfactant strongly affects particle size and morphology of nanoparticles obtained. The reaction is followed by continuous stirring to keep homogeneity in the system. Furthermore, adjusting NaOH as a precipitating agent to a precursor solution has proven to initiate the precipitation. Several phenomena occur in that process, i.e. adsorption on particle surfaces and trapping occlusion of foreign substances during rapid crystal growth. The process occurring in the synthesis of $NdNiO_3$ perovskite nanoparticles could be described with the following stoichiometric chemical equations.

$$Nd(NO_3)_3 + Ni(NO_3)_2 + 5\ NaOH \rightarrow Nd(OH)_3 + Ni(OH)_2 + 5\ NaNO_3 \quad (1)$$

$$2\ Nd(OH)_3 + 2\ Ni(OH)_2 \rightarrow Nd_2O_3 + 2\ NiO + 5\ H_2O \textit{ (heating stage 1)} \quad (2)$$

$$Nd_2O_3 + 2\ NiO + \tfrac{1}{2}\ O_2 \rightarrow 2\ NdNiO_3 \textit{ (heating stage 2)} \quad (3)$$

The final product of the reactions (Reaction 1) was separated using a fluid-solid separation operation by the centrifugation method. Centrifugation was very effective in increasing sedimentation rates, especially when the particles were very small (<10 mm), the liquid was very viscous, and the differences in density between particles and liquids were very small [38]. The

first precipitates formed were a mixture of $Nd(OH)_3$ and $Ni(OH)_2$. Washing process to these precipitates with water and ethanol was to remove the unreacted molecules and get the products free from sodium and nitrates species as well as an excess of surfactant.

At the first heating stage, drying process, the hydroxide compounds were changed to the oxide compounds, Nd_2O_3 and NiO, with a temperature 1 = 100 °C (Reaction 2). The metal hydroxides decomposed to the oxides and transformed to the perovskites at high calcination temperature. The products were then ground into a powder which still contain some associated water and it was removed by heating stage 2. The heating was then ignited by calcination at different temperatures, 700 °C and 900 °C (Reaction 3). At this stage, Ni^{2+} underwent oxidation to Ni^{3+} by oxygen as the temperature increases to be constant. The calcination process was done to remove volatile compounds and form nanosized crystalline phase. The results of that process were $NdNiO_3$ perovskite nanoparticles.

X-ray Diffractometer

Figure 2 showed the XRD pattern of materials obtained along synthesis calcined at different temperatures. The intensity of the peaks changed with calcinations temperature. The as-synthesis products calcined at 900 °C (P900) indicated the formation of a crystalline phase of $NdNiO_3$ nanoparticles, ABO_3 perovskite-type. Otherwise, peaks corresponding to additional oxides phases attributed to very intense peaks such as Nd_2O_3, NiO, Nd_2NiO_4 were also found at that temperature. In the case of the synthesis product calcined at 700 °C (P700), the hydroxide and oxide phases were clearly formed, i.e. $Nd(OH)_3$, $Ni(OH)_2$, Nd_2O_3, NiO, and Nd_2NiO_4. At the heating stage 1 (Reaction 2), the metal hydroxides were predicted not completely decomposed to the oxides and may be transformed to the perovskites at very high calcination temperature. It may be caused by the short duration of heating stage 1 which is only for 1 h. At the temperatures lower than 900 °C, there are no $NdNiO_3$ nanoparticles formed. Therefore, XRD analysis confirmed that P900 was much better than P700 due to its result that produces perovskite and no hydroxide compounds.

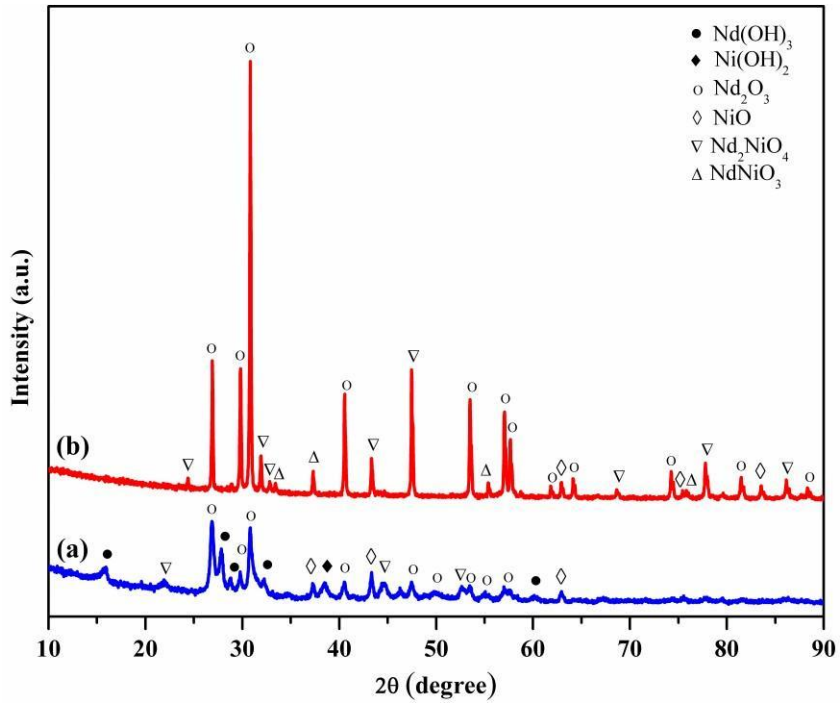

Figure 2: XRD pattern of the materials obtained along synthesis calcined at (a) 700 °C and (b) 900 °C The ABO_3 perovskite-type structure was detected only at 900 °C. The perovskite structure of $NdNiO_3$ in P900 was confirmed peaks by intense reflections in 2θ equal to 33.40°,

37.30°, 55.38°, and 75.84° with a high degree of crystallinity. Additional analysis of the XRD patterns estimated that the average crystallite size of $NdNiO_3$ at these four peaks was ranging between 44–72 nm using Debye-Scherrer formula (Equation 1). The obtained $NdNiO_3$ formed in the orthorhombic structure with the lattice constant a = 5.377 Å, b = 5.394 Å, and c = 7.612 Å which are very close, in good agreement, to the previous report for the $NdNiO_3$ materials [39,40,41]. The variation of crystallite size of the $NdNiO_3$ perovskite nanoparticles in P900 was summarized in Table 1. The lattice interplanar spacing of the crystal was also showed using Bragg's law [42].

Table 1: Various parameters of $NdNiO_3$ perovskite nanoparticles correspond to P900's XRD pattern

Peak position	**FWHM**	**Interplanar spacing**	**Crystallite size**
2θ **[°]**	***β*** **[°]**	***d-spacing*** **[nm]**	D_{XRD} **[nm]**
33.40	0.19	0.27	44.29
37.30	0.12	0.24	67.16
55.38	0.12	0.17	71.86
75.84	0.19	0.13	53.77

The interesting one of this work is the presence of intermediate phases, Nd_2NiO_4 structure, in both P700 and P900. As-synthesis of $LaNiO_3$ perovskites reported by Yang et al. [43], the perovskite phase could be regenerated from metal or oxides. In this study, the result reported that $NdNiO_3$ phase was regenerated from Nd_2NiO_4 intermediate phase and NiO oxide phase in air atmosphere. It occurred during the calcination process, because Nd_2NiO_4 and NiO were detected before the formation of perovskite structure at 900 °C. The Nd_2NiO_4 may be formed as intermediate, since Nd_2NiO_4 phases were also detected both at P700 and P900. The formation of perovskite phases from intermediate phases can be described in the chemical equations as follows.

$$Nd_2O_3 + NiO \rightarrow Nd_2NiO_4 \quad (4)$$

$$Nd_2NiO_4 + NiO + \tfrac{1}{2}\,O_2 \rightarrow 2\,NdNiO_3 \quad (5)$$

The elimination of reactions above corresponded to Reaction 3. The presence of Nd_2NiO_4 and NiO led to the formation of $NdNiO_3$ perovskite structure. The process involved the metal-to-metal transition in these phases. As the temperature rose and kept at calcination temperature, the oxidation state in Nd_2NiO_4 was changed from Ni^{2+} to the Ni^{3+} in $NdNiO_3$ under air atmosphere.

Fourier transform infrared spectrometer

FTIR was carried out to the samples before and after calcination. It was in order to able to compare successful or not removing unwanted functional group from impurities. Also, the broad band of Ni–O stretching vibration and O–Ni– O bending vibration were wanted to detect. The functional groups in nitrate ion as precursors, N═O, as well as in PEG 400 as a surfactant, such as O–H, C–H, and C–O, should disappear after calcination. The empty of these functional group indicated the purity of product. The PEG structure was shown in Figure 3.

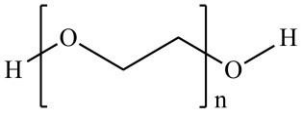

Figure 3: Chemical structure of polyethylene glycol

The FTIR spectra of the PEG 400 and product before as well as after calcination were shown in Figure 4. The PEG spectra showed the absorption peaks at 3432 cm^{-1}, 2866 cm^{-1}, 1092 cm^{-1}, and 1066 cm^{-1} were assigned for O–H broad stretching (alcohol), C–H stretching (alkane), C–O stretching (aliphatic ether), and C–O stretching (primary alcohol) vibrations, respectively. As increasing calcination temperature, the O–H stretching vibrations was gradually got lost and not detected for P900 spectra, as well as on C–H stretching and C–O stretching vibrations.

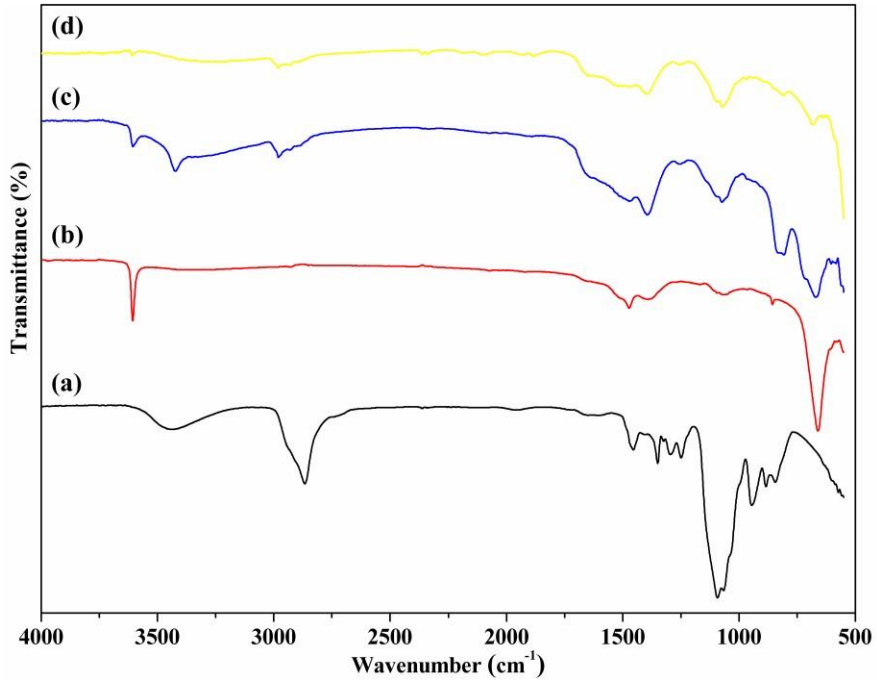

Figure 4: FTIR spectra of (a) PEG 400, (b) product before calcination, (c) P700, and (d) P900

Metal oxides such as Ni–O, provide absorption peak below 800 cm^{-1} due to the inter-atomic vibrations. The broad absorption in the range of 600–700 cm^{-1} is attributed to Ni–O stretching vibration mode [44]. Furthermore, the absorption peak at about 634 cm^{-1} can be assumed to the M–O, O–M–O, and M–O–M (M = Ni, Co) vibrations [45]. The FTIR spectra showed that the Ni–O stretching vibrations were detected in product before and after calcination. In the product before calcination, the Ni–O stretching was led to $Ni(OH)_2$ formed in its precipitate. The assume was also supported by O–H stretching detected at that phase. Moreover, a small amount of $Ni(OH)_2$ was detected in

P700, proved by weak O–H stretching besides of O–Ni–O vibrations in Nd_2NiO_4 compounds. On the other hand, the O–Ni–O vibration in P900 was led to $NdNiO_3$ perovskite nanoparticles. All these assigning proved the formation of $NdNiO_3$ which is in accordance with the XRD characterization.

Surface Area analyzer

To further conceive the nature and geometry of the pores, BET adsorption–desorption isotherm and BJH pore size desorption were conducted in this discussion. The surface area was determined by BET method while pore volume was by BJH method, as presented in Figure 5. The presence of the narrow hysteresis loop was due to the pore nature of the material [46]. The adsorption curves showed multilayer formation for all of the materials as observed in Figures 5a and 5c. The multilayer formation represented stronger interaction compared to both adsorbate and adsorbent surfaces. The BJH pore volume distribution was mainly valid in the range of mesopores–

micropores diameter. It was rather broad with pore volume of about ~1.6 nm (Figures 5b and 5d). As increasing calcination temperatures, the increase in pore radius indicated swelling of the particles.

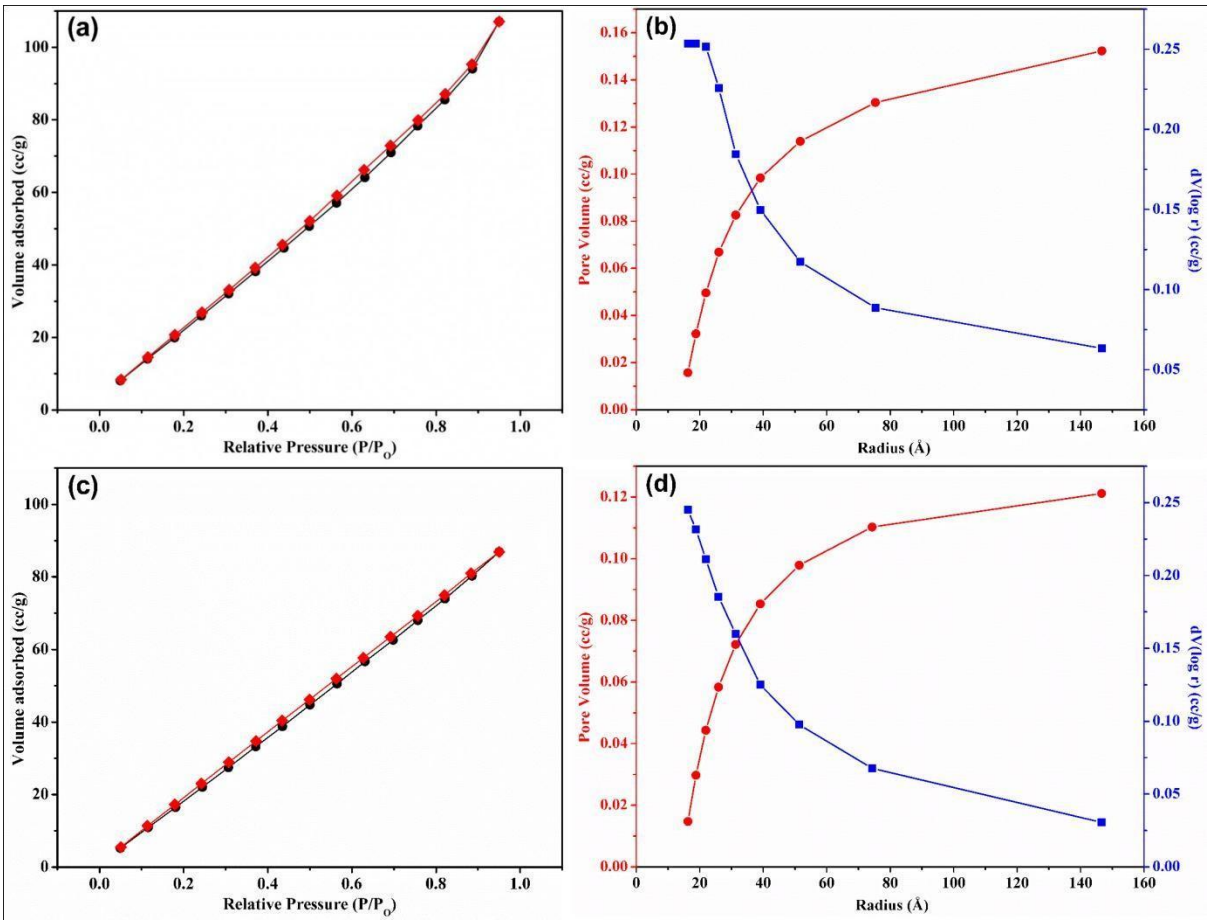

Figure 5: BET surface area sorption isotherm and BJH pore size desorption curve for P700 (a, b) and P900 (c, d) The sample calcined at 900 °C presented surface area which is greater than that calcined at 700 °C. The analysis suggested that $NdNiO_3$ perovskite nanoparticles in P900 have the highest BET specific surface area at 133.79 $m^2 g^{-1}$, with a BJH pore volume of 0.121 cc g^{-1}. A slight decrease in a surface area (130.10 $m^2 g^{-1}$) was observed with a pore volume of 0.152 cc g^{-1} for P700. The data indicated that there is no tendency to form agglomerates as well as the $NdNiO_3$ nanoparticles have smooth surfaces and pores with relatively good width. The detail surface area and pore volume values from the SAA for the materials based on the N_2 sorption isotherm technique were evaluated in Table
2.

Table 2: Surface properties of P700 and P900 from surface area analysis

Sample	Surface area	Pore volume	Pore radius
	***SBET* [m2 g-1]**	***VBJH* [cc g-1]**	**R_{BJH} [Å]**
P700	130.10	0.15	16.25
P900	133.79	0.12	16.27

In this present work, the value of specific surface area of $NdNiO_3$ perovskite nanoparticles via coprecipitation method was a novelty fine particles, also when compared with the typical high temperature $NdNiO_3$ perovskites as well as different synthesis method, i.e. 2–7 $m^2\ g^{-1}$ via pechini method [20]. The other works with different methods to synthesize $NdNiO_3$ have not presented surface area values. As reported by this work, the synthesis of $NdNiO_3$ via coprecipitation method provided a high surface area. The surface area could be attributed to this method be able to produce a perovskite with nanosized particles.

The particle size derived from the BET analysis could be calculated using the equation $D_{BET} = 6/(\rho S)$, proposed by Garvie [47]. For comparison, Table 3 reported crystallite size obtained from XRD analysis using Equation 1 and particle size values from BET analysis.

Table 3: Crystallite and particle sizes of P700 and P900

Sample	Crystallite size	Particle size
	D_{XRD} [nm]	D_{BET} [nm]
P700	24.49	6.11
P900	63.01	14.10

As evident from table, the result showed similar trend. That is consistent as the temperature in the calcination process was increased, average particle size was significantly getting much larger.

Conclusion

We have conducted a work to synthesize $NdNiO_3$ nanoparticles with an orthorhombic perovskite structure via coprecipitation method with sodium hydroxide as a precipitating agent and polyethylene glycol as a surfactant. The perovskite products are obtained by calcining at 900 °C for 4 h. The crystallite size of $NdNiO_3$ measured by XRD using Scherrer equation shows the nanosized particles in ranging of 44–72 nm. The FTIR analysis indicates O–Ni–O vibration led to $NdNiO_3$ perovskite nanoparticles, in products calcined at 900 °C, with the wavenumber of 634 cm^{-1}. The particle parameters of $NdNiO_3$ nanoparticles are calculated by BET method with a surface area of 133.79 $m^2\ g^{-1}$ as well as by BJH method with a pore volume of 0.121 cc g^{-1}. The results show that the synthesis of $NdNiO_3$ via coprecipitation method is a suitable method to produce fine surfaces and pores with nanosized particles. However, this method forms several unwanted phases.

References

[1]. Kaur, D., Jesudasan, J., & Raychaudhuri, P. (2005). Pulsed laser deposition of $NdNiO_3$ thin films. *Solid State Communications*, *136*(6):369–374.

[2]. Doan, T. D., Abramowski, C., & Salvador, P. A. (2001). Stability and structural characterization of epitaxial $NdNiO_3$ films grown by pulsed laser deposition. *Materials Research Society Symposium - Proceedings*, *658*:1–6.

[3]. Onozuka, T., Chikamatsu, A., Katayama, T., Hirose, Y., Harayama, I., Sekiba, D., … Hasegawa, T. (2017).
Reversible Changes in Resistance of Perovskite Nickelate $NdNiO_3$ Thin Films Induced by Fluorine Substitution. *ACS Applied Materials and Interfaces*, *9*(12):10882–10887.

[4]. Vassiliou, J. K., Hornbostel, M., Ziebarth, R., & Disalvo, F. J. (1989). Synthesis and properties of NdNiO3 prepared by low-temperature methods. *Journal of Solid State Chemistry*, *81*(2):208–216.

[5]. Hooda, M. K., & Yadav, C. S. (2016). Electronic properties and the nature of metal-insulator transition in $NdNiO_3$ prepared at ambient oxygen pressure. *Physica B: Condensed Matter*, *491*:31–36.
[6]. Hu, C., Wang, X., Yao, T., Gao, T., Han, J., Zhang, X., & Song, B. (2019). Enhanced Electrocatalytic Oxygen Evolution Activity by Tuning Both the Oxygen Vacancy and Orbital Occupancy of B-Site Metal Cation in $NdNiO_3$. *Advanced Functional Materials*, *29*(30):1–8.
[7]. Medarde, M. L. (1997). Structural, magnetic and electronic properties of $RNiO_3$ perovskites (R = rare earth). *Journal of Physics: Condensed Matter*, *9*(8):1679.
[8]. Fort, A., Bertocci, F., Mugnaini, M., Rocchi, S., Spinicci, R., & Vignoli, V. (2012). Preparation and Characterization of CO Sensors based on Pd modified $YCoO_3$ Perovskite, 8–11.
[9]. Sivakumar, M., Pandi, K., Chen, S. M., Cheng, Y. H., & Sakthivel, M. (2017). Facile synthesis of perovskite-type $NdNiO_3$ nanoparticles for an effective electrochemical non-enzymatic glucose biosensor. *New Journal of Chemistry*, *41*(19): 11201–11207.
[10]. Jun, A., Kim, J., Shin, J., & Kim, G. (2016). Perovskite as a Cathode Material: A Review of its Role in Solid-Oxide Fuel Cell Technology. *ChemElectroChem*, *3*(4):511–530.
[11]. Wang, K., Song, J., Duan, X., Mu, J., & Wang, Y. (2017). Perovskite $LaCoO_3$ nanoparticles as enzyme mimetics: Their catalytic properties, mechanism and application in dopamine biosensing. *New Journal of Chemistry*, *41*(16):8554–8560.
[12]. Liu, Y., Ma, J., Lai, J., & Liu, Y. (2009). Study of $LaCoO_3$ as a cathode catalyst for a membraneless direct borohydride fuel cell. *Journal of Alloys and Compounds*, *488*(1):204–207.
[13]. Wu, L., Zhu, Y., Park, S., Shapiro, S., Shirane, G., & Tafto, J. (2005). Defect structure of the highdielectric-constant perovskite $CaCu_3Ti_4O_{12}$. *Physical Review B - Condensed Matter and Materials Physics*, *71*(1):1–7.
[14]. Harikrishnan, M. P., & Bose, A. C. (2019). $LaNiO_3$ perovskite oxides by co-precipitation method as electrode for high performance supercapacitor. *AIP Conference Proceedings*, *2115*(July):3–7.
[15]. Sahoo, S. K., Manoharan, B., & Sivakumar, N. (2018). Introduction: Why Perovskite and Perovskite Solar Cells? In *Perovskite Photovoltaics*, Elsevier Inc., Amsterdam, 1–24.
[16]. Mesquita, I., Andrade, L., & Mendes, A. (2018). Perovskite solar cells: Materials, configurations and stability. *Renewable and Sustainable Energy Reviews*, *82* (September 2017): 2471–2489.
[17]. Tan, R., Zhu, Y., Feng, J., Ji, S., & Cao, L. (2002). Preparation of nanosized $LaCo_xMn_{1-x}O_3$ perovskite oxide using amorphous heteronuclear complex as a precursor. *Journal of Alloys and Compounds*, *337*(1– 2):282–288.
[18]. Ignatius, A. S., Peter, P. R. A., & John, B. L. (2012). Synthesis and Characterisation of Nano crystalline Neodymium Nickelate ($NdNiO_3$) Powders using Low Temperature Molten Salt Technique. *Research Journal of Chemical Sciences*, *2*(8):37–42.
[19]. Fujihara, S., Kozuka, H., & Yoko, T. (1994). Structure, Oxygen Deficiency and Electrical Properties of $Nd_{1-x}Y_xNiO_{3-y}$ (x=0, 0.1) Prepared by Sol-Gel Method. *Journal of the Ceramic Society of Japan*, *102*(11):1005–1009.

[20]. Fernandes, J. D. G., Araújo Melo, D. M., Zinner, L. B., Salustiano, C. M., Silva, Z. R., Alves Júnior, C., & Longo, E. (2002). Synthesis and characterization of neodymium nickelate powder produced from polymeric precursors. *Journal of Alloys and Compounds*, *344*(1–2):157–160.

[21]. Capon, F., Horwat, D., Pierson, J. F., Zaghrioui, M., & Laffez, P. (2009). Thermochromic effect in $NdNiO_{3-\delta}$ thin films annealed in ambient air. *Journal of Physics D: Applied Physics*, *42*(18).

[22]. Oliveira, R. M. P. B., Pimentel, P. M., Araújo, J. H., Melo, D. M. A., Melo, M. A. F., & Martinelli, A. E. (2013). Microstructural study of neodmium nickelate doped with strontium synthesized by gelatin method.
Advances in Materials Science and Engineering, *2013*.

[23]. Ferkhi, M., Rekaik, M., Khaled, A., Cassir, M., & Pireaux, J. J. (2017). Neodymium nickelate $Nd_{2-x}Sr_xNi_{1}yCo_yO_{4\pm d}$ (x and y = 0 or 0.05) as cathode materials for the oxygen reduction reaction. *Electrochimica Acta*, *229*:281–29.

[24]. Nakayama, S. (2001). $LaFeO_3$ perovskite-type oxide prepared by oxide-mixing, co-precipitation and complex synthesis methods. *Journal of Materials Science*, *36*(23):5643–5648.

[25]. Chandradass, J., Kim, H., & Momade, F. W. Y. (2014). Effect of different solvents in the synthesis of $LaCoO_3$ nanopowders prepared by the co-precipitation method. *Advanced Powder Technology*, *25*(6):1834–1838.

[26]. Zhang, C., Guo, Y., Guo, Y., Lu, G., Boreave, A., Retailleau, L., Giroir-Fendler, A. (2014). $LaMnO_3$ perovskite oxides prepared by different methods for catalytic oxidation of toluene. *Applied Catalysis B: Environmental*, *148–149*:490–498.

[27]. Djoudi, L., Omari, M., & Madoui, N. (2012). Synthesis and characterization of lanthanum monoaluminate by co-precipitation method. *EPJ Web of Conferences*, *29*.

[28]. Prakash, B. J., Kumar, K. N., & Buddhudu, S. (2012). Thermal, magnetic and electrical properties of multiferroic $GdMnO_3$ nano particles by a co-precipitation method. *Ferroelectrics, Letters Section*, *39*(4– 6):104–116.

[29]. Khorasani-Motlagh, M., Noroozifar, M., Yousefi, M., & Jahani, S. (2013). Chemical Synthesis and Characterization of Perovskite $NdFeO_3$ Nanocrystals via a Co-Precipitation Method. *International Journal of Nanoscience and Nanotechnology*, *9*(1):7–14.

[30]. Rane, A. V., Kanny, K., Abitha, V. K., & Thomas, S. (2018). *Methods for Synthesis of Nanoparticles and Fabrication of Nanocomposites*. *Synthesis of Inorganic Nanomaterials*, Elsevier Ltd., Amsterdam.

[31]. Lima-Tenório, M. K., Gómez Pineda, E. A., Ahmad, N. M., Fessi, H., & Elaissari, A. (2015). Magnetic nanoparticles: In vivo cancer diagnosis and therapy. *International Journal of Pharmaceutics*, *493*(1– 2):313–327.

[32]. Wu, W., Jiang, C. Z., & Roy, V. A. L. (2016). Designed synthesis and surface engineering strategies of magnetic iron oxide nanoparticles for biomedical applications. *Nanoscale*, *8*(47):19421–19474.

[33]. Nawaz, M., Sliman, Y., Ercan, I., Lima-Tenório, M. K., Tenório-Neto, E. T., Kaewsaneha, C., & Elaissari, A. (2019). *Magnetic and pH-responsive magnetic nanocarriers*. *Stimuli Responsive Polymeric Nanocarriers for Drug Delivery Applications*. Elsevier Ltd., Amsterdam.

[34]. Cullity, B. D., & Stock, S. R. (2014). *Elements of X-Ray Diffraction*. *Pearson*, Pearson, Essex, 3rd ed.

[35]. Brunauer, S., Emmett, P. H., & Teller, E. (1938). Adsorption of Gases in Multimolecular Layers. *Journal of the American Chemical Society*, *60*(2):309–319.
[36]. Barrett, E. P., Joyner, L. G., & Halenda, P. P. (1951). The Determination of Pore Volume and Area Distributions in Porous Substances. I. Computations from Nitrogen Isotherms. *Journal of the American Chemical Society*, *73*(1):373–380.
[37]. Damisih, Raharjo, J., Yuliani, H., Hapsari, A. U., Masmui, Pravitasari, R. D., & Grandevi. (2019). Effect polyethylene glycol (PEG 400) to the physical properties of gadolinium doped cerium ($Ce_{0.9}Gd_{0.1}O_{1.95}$) nanoparticles synthesized by co-precipitation method. *IOP Conference Series: Materials Science and Engineering*, *622*:1–13.
[38]. Seader, J. D., Henley, E. J., & Roper, D. K. (2011). *Separation Process Principles-Chemical and Biochemical Operations*, John Wiley & Sons Inc., 3rd ed.
[39]. Lacorre, P., Pannetier, J., Nazzal, S. A. I., Wang, P. W., & Huang, T. C. (1991). P. lacorre,j. b. torrance, j. pannetier, s. a. i. nazzal, p. w. wang. *Journal of Solid State Chemistry*, *237*:225–237.
[40]. García-Muñoz, J. L., Rodríguez-Carvajal, J., Lacorre, P., & Torrance, J. B. (1992). Neutron-diffraction study of $RNiO_3$ (R=La, Pr, Nd, Sm): Electronically induced structural changes across the metal-insulator transition. *Physical Review B*, *46*(8):4414–4425.
[41]. Blasco, J., Castro, M., & Garcia, J. (1994). Structural, electronic, magnetic and calorimetric study of the metal-insulator transition in $NdNiO_3$- delta. *Journal of Physics: Condensed Matter*, *6*(30):5875–5889.
[42]. West, A. R. (2014). *Solid State Chemistry and its Applications*, John Wiley & Sons Inc., West Sussex, 2nd ed.
[43]. Yang, E. hyeok, & Moon, D. J. (2016). Synthesis of $LaNiO_3$ perovskite using an EDTA-cellulose method and comparison with the conventional Pechini method: application to steam CO_2 reforming of methane. *RSC Advances*, *6*(114):112885–112898.
[44]. Wei, Z., Qiao, H., Yang, H., Zhu, L., & Yan, X. (2009). Preparation and characterization of NiO nanoparticles by anodic arc plasma method. *Journal of Nanomaterials*, *2009*.
[45]. Li, R., Hu, Z., Shao, X., Cheng, P., Li, S., Yu, W., … Yuan, D. (2016). Large scale synthesis of NiCo layered double hydroxides for superior asymmetric electrochemical capacitor. *Scientific Reports*, *6*(January):1–9.
[46]. Nayak, N. B., & Nayak, B. B. (2016). Temperature-mediated phase transformation, pore geometry and pore hysteresis transformation of borohydride derived in-born porous zirconium hydroxide nanopowders. *Scientific Reports*, *6*(October 2015):1–11.
[47]. Garvie, R. C. (1965). The occurrence of metastable tetragonal zirconia as a crystallite size effect. *Journal of Physical Chemistry*, *69*(4):1238–1243.